ACS OMEGA

http://pubs.acs.org/journal/acsodf

Article

Covalently Functionalized Graphene with Molecularly Imprinted Polymers for Selective Adsorption and Electrochemical Detection of Chloramphenicol

Thi Nhat Thang Nguyen, Nam Thi Pham, Dai-Hung Ngo, Subodh Kumar,* and Xuan Thang Cao*

Cite This: *ACS Omega* 2023, 8, 25385−25391

Read Online

ACCESS | Metrics & More | Article Recommendations | Supporting Information

ABSTRACT: In this report, we have presented a novel route to attach molecularly imprinted polymers (MIPs) on the surface of reduced graphene oxide (rGO) through covalent bonding. First, the surface of rGO was modified with maleic anhydride (MA) *via* a Diels−Alder reaction using a deep eutectic solvent (DES). Next, 3-propyl-1-vinylimidazolium molecular units were anchored and polymerized in the presence of ethylene glycol dimethacrylate (EGDMA) using chloramphenicol (CAP) as the template. Primarily, we investigated the effect of the molar ratio of individual precursors on the adsorption capacity of synthesized materials and accordingly fabricated the electrochemical sensor for CAP detection. Electrochemical results evidenced that the covalent bonding of MIP units enhanced the sensitivity of the respective sensor toward CAP in water as well as in real honey samples with high selectivity, stability, and reproducibility. This synthesis strategy involves the covalent binding of MIP on rGO materials *via* click chemisty under sonication power excluding harmful solvents and energy-intensive processes and thus could be a motivation for developing future electrochemical sensors through similar "green" routes.

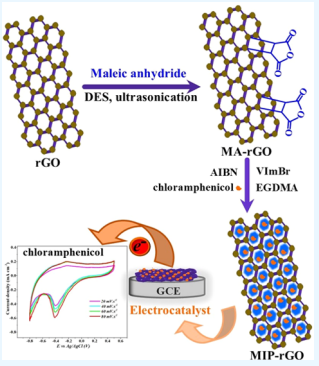

1. INTRODUCTION

Chloramphenicol (CAP), an antibiotic, has been widely used for the treatment of typhoid fever and other diseases in animals as it can inhibit bacterial protein synthesis.[1,2] However, it has shown some harmful side effects to food-producing animals and consequently been banned to prevent possible transmission of its persistence to the human body.[3−5] In fact, accumulation of CAP in the human body even at low concentrations can not only cause sickness (nausea, vomiting, diarrhea, bone marrow suppression, aplastic anemia, leukemia) but also induce liver- and kidney-related problems.[6] Therefore, it is quite essential to detect even a trace amount of CAP in biological and food products. Consequently, detection of CAP residues in food industries[7] has been performed by using photoelectrochemical methods,[8,9] surface-enhanced Raman spectroscopy (SERS),[10] amperometric biosensors,[11] fluorescent sensors,[12,13] gas chromatography−mass spectrometry (GC-MS),[14] and liquid chromatography−tandem mass spectrometric (LC-MS/MS) techniques.[15] However, most of these methods are expensive in nature and require specific expertise. Hence, the ideas of developing simple and comparatively low-cost detection methods are always attractive. MIPs are a noble class of polymers with enhanced adsorption as well as detection properties for a particular solute. In fact, molecularly imprinted polymers (MIPs) have been utilized for the selective determination of CAP.[16−18] Moreover, molecularly imprinted polymer (MIP)-based electrochemical sensors have also been utilized as great alternatives due to their fast and easy preparation, comparatively low cost, effectiveness, and simple application.[17,19] The working principle of MIP-based electrochemical sensors is based on the quenching of current and peak voltage during analyte binding due to the occurrence of oxidation and reduction processes at the MIP-based electrode. Synthesis of MIP generally involves two steps: (1) cross-linking polymerization of the functional monomer in the presence of desired template molecules; and (2) removal of the template from the cross-linked polymer matrix. In this process, the resulting polymer comprises a complementary three-dimensional (3D) imprint of the used template. This specific feature of MIP is responsible for high selectivity in terms of adsorption and sensitivity toward the respective template molecule.[20] However, bare MIP-based electrochemical sensors exhibit a comparatively low activity due to slow binding kinetics, less conductivity, and limited adsorption capacity. Therefore, MIPs are generally integrated with other conductive and porous nanomaterials with the aim to improving their efficiency as electrochemical sensors. Moreover, the integration process may enhance the accessibility of adsorption sites by limiting the overpolymerization to prevent the burial of active sites deep inside the polymeric layer. Graphene derivative-based nanocomposites have been receiving much attention for

Received: April 25, 2023
Accepted: June 23, 2023
Published: July 5, 2023

Scheme 1. Stepwise Synthesis of MIP-rGO

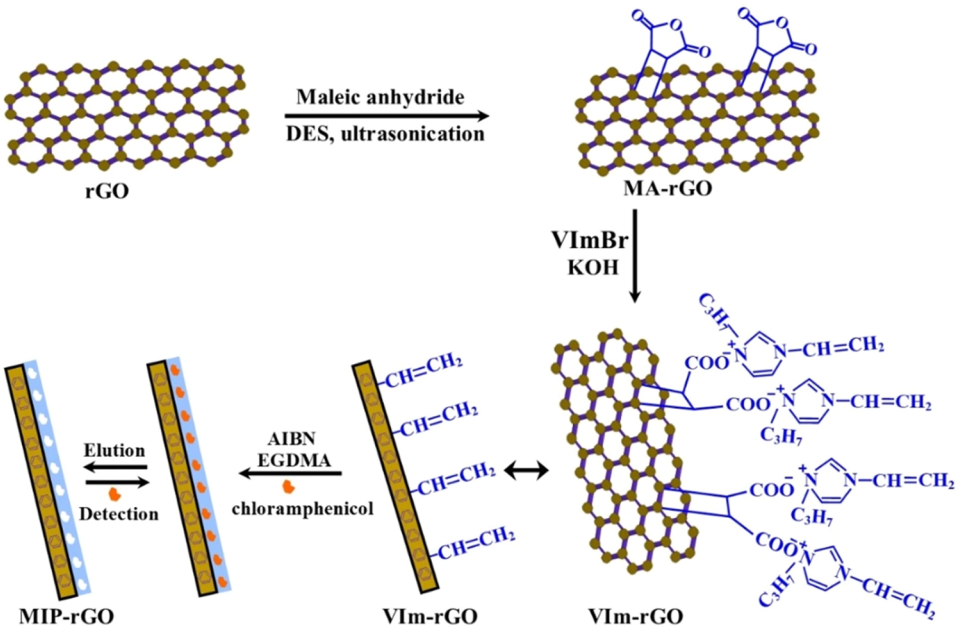

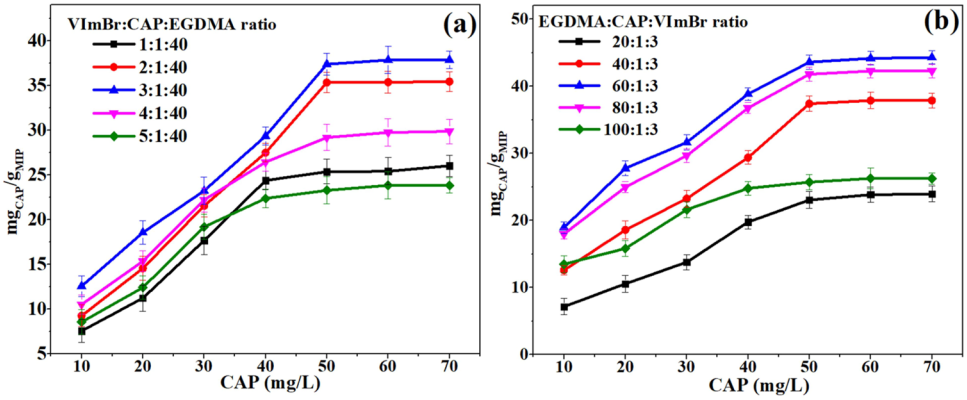

Figure 1. Adsorption capacity of MIP-rGO materials synthesized using different molar ratios of (a) VImBr:CAP:EGDMA and (b) EGDMA:CAP:VImBr.

numerous applications in electrocatalysis including electrochemical sensors. In addition to other specific features, the high electrical conductivity of graphene derivatives makes them demanding associate materials to enhance the electrochemical activity of the resulting nanocomposites.[21−24] The properties of the nanocomposites also depend on their synthesis processes. Therefore, many methods have been proposed for developing MIP-based graphene materials such as laser-induced graphene technique,[25] laser scribed graphene (LSG) technology,[26] and chemiluminescence resonance energy transfer (CRET) principle.[27] Moreover, the activity also depends on the type of interaction (physical or chemical) between the comaterials of nanocomposites. It has been reported that covalently bonded active sites (metallic or nonmetallic species) onto the surface of graphene derivatives exhibited a higher stability and sensitivity and facilitated the electron transfer reactions.[28,29] However, covalent functionalization of graphene derivatives generally involves prior modification of their surface *via* chemical processes. The Diels−Alder reaction is one of the advanced methods for the modification of the graphitic surface by leveraging the presence of C=C bonds. Generally, this process requires harmful solvents and severe reaction conditions, thus limiting its applications.[30,31] Thanks to deep eutectic solvents (DESs), they have been explored as green reaction mediums for performing the Diels−Alder reaction at ambient conditions.[32,33]

In this work, we have prepared covalently functionalized molecularly imprinted polymers onto the surface of reduced graphene oxide (rGO). DESs allowed a facile surface modification of rGO under environment-friendly conditions without involving any harmful solvents and reagents. The covalently bonded MIP-based graphene nanocomposite was tested for the adsorption and electrochemical detection of CAP in water and real honey samples. Nevertheless, to the best of our knowledge, synthesis routes for the preparation of MIP-based graphene materials involving DESs have not been reported to date.

2. RESULTS AND DISCUSSION

2.1. Synthesis and Characterization. Synthesis processes involve the modification of the rGO surface first with maleic anhydride (MA) *via* the Diels−Alder reaction in DES

https://doi.org/10.1021/acsomega.3c02839
ACS Omega 2023, 8, 25385−25391

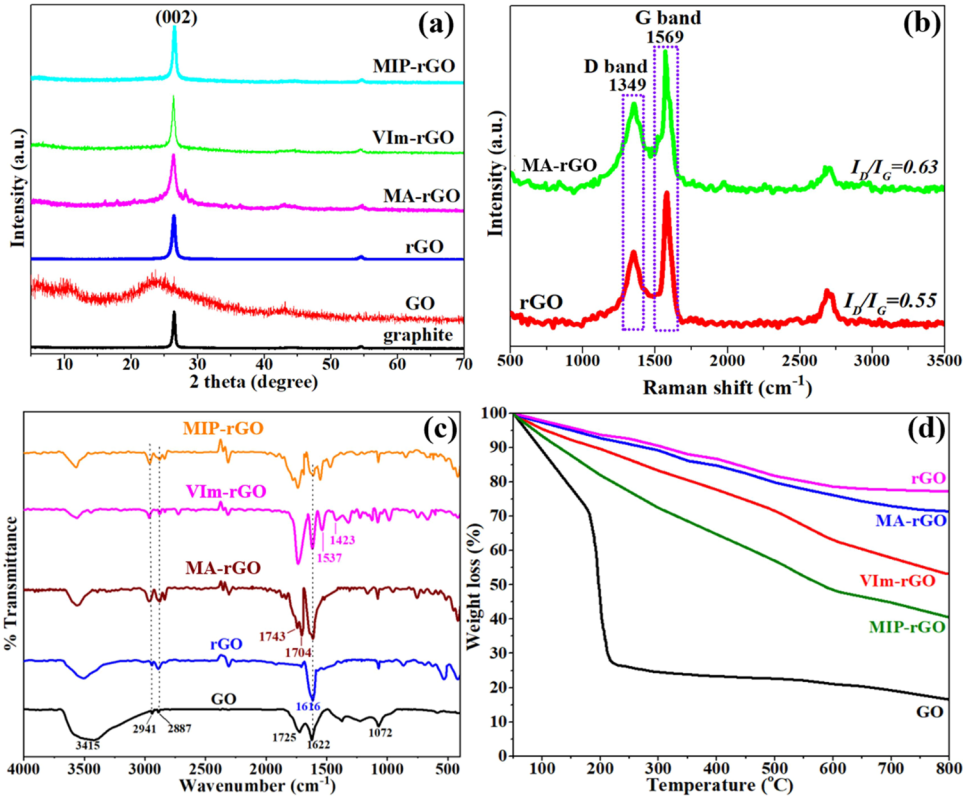

Figure 2. (a) X-ray diffraction patterns of GO, rGO, MA-rGO, VIm-rGO, and MIP-rGO; (b) Raman spectra of rGO and MA-rGO; (c) Fourier transform infrared (FTIR) spectra; and (d) thermogravimetric analysis (TGA) curves of GO, rGO, MA-rGO, VIm-rGO, and MIP-rGO.

under ultrasonication assistance. Next, 3-propyl-1-vinylimidazolium bromide (VImBr) molecular species were anchored and then polymerized in the presence of a CAP template using ethylene glycol dimethacrylate (EGDMA) as a cross-linker. Finally, MIP-functionalized rGO (MIP-rGO) was obtained on removal of the template molecule (Scheme 1).

Primarily, the adsorption capacity of MIP-rGO nanocomposites was evaluated as it is one of the most important features to determine their effectiveness. For this, we also prepared some other MIP-rGO nanocomposites using different molar ratios of CAP, VImBr, and EGDMA to investigate the role of their composition in achieving the optimum adsorption capacity. Experimentally, MIP-rGO nanocomposites were dispersed in water solutions of CAP of different strengths under constant stirring at room temperature for 24 h. Next, the filtrate was collected and reconstituted in an acetonitrile/buffer solution for HPLC analysis to quantify the CAP concentration. The adsorption capacity of the respective materials was found to increase as the molar ratio of VImBr and EGDMA increases with respect to CAP and reaches the maximum at 3:1 and 60:1 molar ratios, respectively (Figure 1). It could be due to the increased number of binding sites because of the precise ratio of VImBr and EGDMA. However, further increase in the molar ratio resulted in a decrease in the adsorption capacity, indicating restricted access of adsorption sites. It could be due to their hiding deep inside under the thick polymer layer formed after consumption of all of the CAP templates. Moreover, the adsorption profile of MIP-rGO toward CAP was investigated as shown in Figure S1. The adsorption increased rapidly in the first 60 min, and equilibrium was reached after 180 min. The maximum adsorption capacity of MIP-rGO with the 60:1:3 molar ratio of EGDMA/CAP/VimBr was found to be 45.68 mg/g and thus was selected as a model catalyst for further characterization and electrochemical experiments.

Crystalline structures of graphite, GO, rGO, MA-rGO, VIm-rGO, and MIP-rGO were examined by X-ray diffraction (XRD) analysis (Figure 2a). Graphite powder showed a sharp reflection at a 2θ value of 26.47° corresponding to the (002) plane with a lattice spacing of 0.336 nm. On the other hand, GO showed two broad peaks at 10.7 and 23.1° 2θ with higher d-spacings of 0.822 and 0.385 nm, respectively, indicating the successful oxidation of graphite powder. However, on heat treatment of GO at 350 °C under an inert atmosphere, peaks vanished at 10.7 and 23.1° and instead a new sharp peak appeared at 26.4° 2θ. This new peak indicates the graphitic nature and restoration of some planarity as a result of elimination of oxygen functional groups from the surface of GO transforming into rGO. A similar peak was observed in the XRD diffraction patterns of MA-rGO, VIm-rGO, and MIP-rGO samples, indicating that the planar structure and crystallinity of rGO were preserved during the covalent functionalization process. Raman spectra were used to examine the structural integrity of MA-rGO to confirm the actual occurrence of the DA reaction between MA and rGO. Two peaks at 1349 and 1569 cm^{-1} corresponding to D and G bands, respectively, were observed (Figure 2b). The intensity ratio (I_D/I_G) of these bands is used as an important factor to measure the defect of the graphitic materials. The I_D/I_G ratios for rGO and MA-rGO were found to be 0.55 and 0.63, respectively. The increase in the I_D/I_G ratio for MA-rGO is a clear indication of a decrease in the number of sp^2 carbons because of the DA click reaction between MA and the diene bond on the surface of rGO.

https://doi.org/10.1021/acsomega.3c02839
ACS Omega 2023, 8, 25385−25391

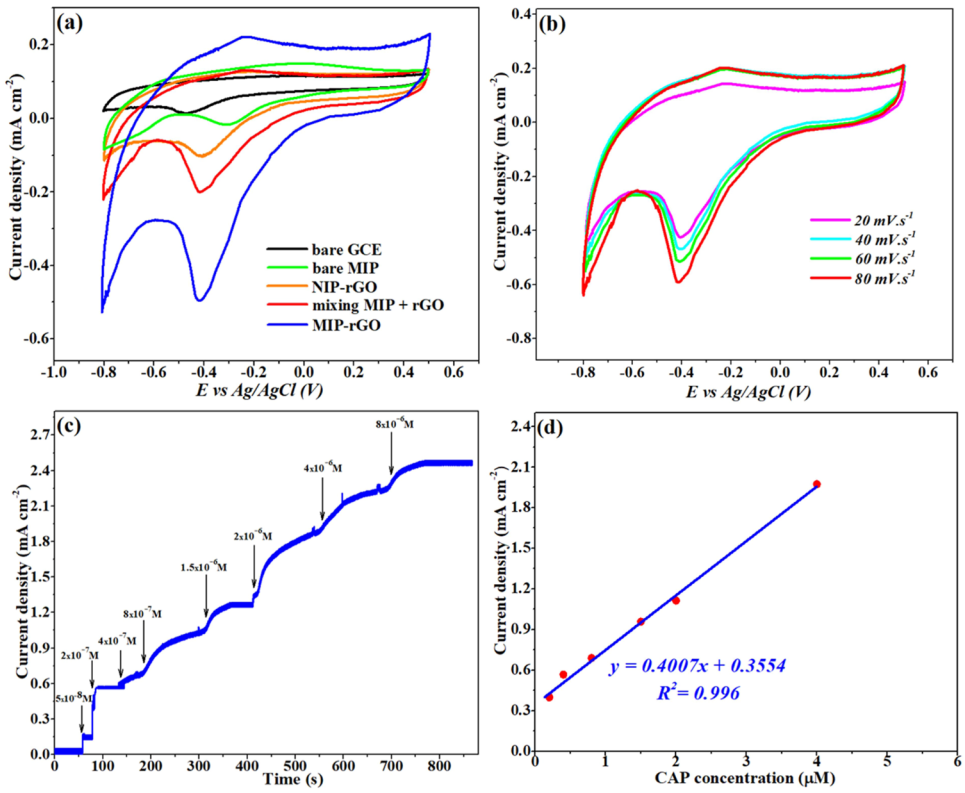

Figure 3. (a) CV graphs of different electrodes at a scan rate of 40 mV/s; (b) CV graph of MIP-rGO at different scan rates: PBS (pH 7.0) with 1×10^{-6} M CAP. (c) Amperometric response upon successive addition of CAP (0.05−8.0 μM) at an applied potential of −0.25 V in PBS (pH 7.0). (d) Linear relation of current with CAP concentration.

FTIR spectra of GO, rGO, MA-rGO, VIm-rGO, and MIP-rGO are depicted in Figure 1c. In the spectrum of GO, typical absorption peaks at 3415 and 1725 cm^{-1} could be ascribed to hydroxyl and carbonyl stretching, while the peaks at 1622 and 1072 cm^{-1} were assigned to C═C and C−O bending, respectively. After the thermal reduction process, the peak intensity of oxygen functional groups in the spectrum of rGO decreased due to the elimination of oxygen functionalities, whereas the aromatic ring stretching at 1616 cm^{-1} increased concurrently. Moreover, the covalent bonding of MA was evident by two additional absorption bands at 1743 and 1704 cm^{-1} corresponding to the C═O vibration of MA and carboxyl groups, respectively. It is well-known that the anhydride group is highly reactive and can be hydrolyzed easily under a basic medium. Therefore, an ionic exchange reaction between MA-rGO and VIm was facilitated in the presence of potassium hydroxide. The FTIR spectrum of VIm-rGO shows characteristic absorption bands of the imidazolium ring at 1537 and 1423 cm^{-1}, indicating the occurrence of an ionic exchange reaction. MIP-rGO was obtained by the polymerization process using EGDMA as a cross-linker, which reduced the respective C═C bonds at 1622 cm^{-1}, confirming the successful formation of polymeric units. The thermal degradation behavior of all of the samples was evaluated *via* TGA in the temperature range of 50−800 °C under a N_2 atmosphere. Weight loss was observed for all of the samples starting around 100 °C due to the removal of moisture and starting of decomposition of oxygen functionalities (Figure 2d). In the cases of MA-rGO and VIm-rGO, further weight loss could be associated with the successive degradation of MA and VIm organic moieties. However, high weight loss was observed in the same temperature range for MIP-rGO due to the decomposition of a large number of organic moieties, thus indicating high loading in the form of polymeric units. Moreover, it could also be due to the evaporation of entrapped organic moieties in the 3D imprint voids generated as a result of template removal. The change in surface morphology after the chemical functionalization was investigated by scanning electron microscopy (SEM) analysis (Figure S2). All of the materials exhibited a layered type of structure, indicating that there was no observable change in the surface morphology during the chemical functionalization process. The nitrogen adsorption−desorption isotherms and pore-size distribution of MIP-rGO are shown in Figure S3. The Brunauer−Emmett−Teller (BET) surface area was measured to be 296.4 m^2/g with a pore size of 4.3 nm. The isotherm appears to be type IV according to the IUPAC definitions and thus indicates the mesoporous nature of the material. Moreover, the formation of pores with a uniform size clearly suggests the involvement of a single-type template, which is CAP. Thus, all of these characterization techniques collectively confirmed the successful synthesis of covalently bonded MIP onto the surface of rGO (MIP-rGO).

2.2. Catalytic Activity. The electrochemical behavior of synthesized MIP-rGO was examined along with bare MIP, NIP-rGO, and a physical mixture of MIP and rGO toward CAP detection in a phosphate-buffered solution (PBS) at pH = 7.0 and a scan rate of 40 mV/s (Figure 3a). It can be seen that the bare glassy carbon electrode exhibited no response, while the NIP-rGO-based electrode displayed a very low response toward CAP due to nonspecific adsorption. Nevertheless, the MIP-rGO-based electrode showed an anode peak at −0.25 V

https://doi.org/10.1021/acsomega.3c02839
ACS Omega 2023, 8, 25385−25391

and two cathode peaks at −0.41 and −0.79 V. This result could be explained by the fact that the oxidation/reduction process occurred on the surface of electrodes. The presence of the peak at −0.79 V is due to the irreversible reduction of the nitro group to the hydroxylamine group, while the peaks at −0.25 and −0.41 V correspond to the reversible redox reaction of the hydroxylamine group, giving the nitroso derivative.[34] The current responses in anodic and cathodic peaks were found to increase with a faster scan rate, indicating the responsive ability of the MIP-rGO-based electrode (Figure 3b). Additionally, the reduction peaks shifted toward a more negative potential at higher scan rates due to the increase in the internal diffusion resistance.[35] Although the physical mixture of MIP and rGO exhibited similar anode and cathode peaks, a comparatively low current response was achieved. Furthermore, bare MIP also failed to perform better, displaying poor response in the form of the current density. These cyclic voltammetry (CV) results validated not only the importance of rGO as a support material but also covalent bonding between MIP and rGO to achieve the optimum electrochemical activity. We further examined the effect of pH on the electrochemical behavior of CAP, and the results demonstrated that the highest current density of the cathodic peak was observed at pH 7.0 (Figure S4). Next, chronoamperometry (CA) was performed upon successive addition of CAP, from 0.05 to 8.0 μM (Figure 3c). It is evident that the current density increased continuously during the addition of CAP and reached a nearly constant stage at 8×10^{-6} M. A linear regression equation was used to model the relationship between the current density and the CAP concentration in the range of 0.2−4.0 μM with correlation coefficient (R^2) 0.996 (Figure 3d). Subsequently, the limit of detection (LOD) and the limit of quantification (LOQ) were calculated from the linear regression equation in Figure 3d, which were found to be 0.204 and 0.619 μM, respectively. Notably, the fabricated sensors presented a comparability higher sensitivity in terms of LOD than the other electrochemical sensors reported in previous studies (Table S1).

High selectivity is the most important feature of MIP materials and is crucial for the detection of desired molecules in the commercial samples. Therefore, we selected *p*-nitrophenol and thiamphenicol as interferences molecules for the evaluation of selectivity toward CAP. The MIP-rGO-based electrochemical sensor demonstrated excellent selectivity in the solution of *p*-nitrophenol and thiamphenicol with a 40-fold higher concentration than CAP (Figure S5). Additionally, relatively low current intensities were obtained in the case of the interferent itself (*p*-nitrophenol or thiamphenicol), illustrating the high sensitivity and selectivity of MIP-rGO toward CAP. Moreover, the applicability of the sensors at the commercial level requires high repeatability and reproducibility. Therefore, the MIP-rGO-based sensor was recycled for five subsequent experiments. It succeeded in retaining 96.2% of the initial current density with a relative standard deviation (RSD) of 2.4% (Figure S6a). Reproducibility was evaluated by fabricating five independent electrodes by following the same procedure and tested for CAP detection. The result indicated that the values of the current intensity were varied with an RSD of 2.35% (n = 5) (Figure S6b). Moreover, the XRD pattern of MIP-rGO after five CV cycles was also examined to observe any changes in the material (Figure S7). XRD spectra of the recycled MIP-rGO presented all of the main peaks at the same position as the fresh MIP-rGO, demonstrating no significant change in its structure. These results were encouraging to evaluate the MIP-rGO-based electrochemical sensor for the possible detection of CAP in the commercial sample. For this, real honey was chosen as a commercial food sample to carry out electrochemical detection. In a typical procedure, CAP and real honey samples were added in different concentrations into deionized water homogeneously. CAP was carefully extracted with ethyl acetate solvent, which was removed by a rotary vacuum evaporator. The remaining material was diluted with phosphate-buffered solution and subjected to CAP detection using MIP-rGO-based electrodes. CAP was successfully detected with the recovery range from 94 to 98.7% in the respective samples of different feed concentrations (Table S2). These findings illustrate the great potential of MIP-rGO-based sensors in the field of food industries.

3. CONCLUSIONS

We have demonstrated an efficient route for the synthesis of covalently bonded MIP onto the surface of rGO *via* the Diels−Alder "click" reaction, ionic exchange, and polymerization reactions. FTIR, XRD, TGA, and Raman spectroscopy collectively have confirmed the successful formation of MIP-rGO, while the change in surface morphology was observed by electron microscopy. MIP-rGO synthesized by using the EGDMA/CAP/VImBr = 60:1:3 molar ratio demonstrated excellent adsorption capacity and thus was selected as a model material to fabricate the electrode for CAP detection. CV results evidenced that the covalent bonding of MIP onto the surface of rGO resulted in enhanced sensitivity of the MIP-rGO-based electrode toward CAP with high selectivity, repeatability, and reproducibility. Moreover, CAP was successfully detected in real honey samples, indicating a reliable electrode material for practical applications. The results indicate that MIP-rGO offers great potential not only for the selective adsorption of CAP but also for electrochemical sensing applications.

4. EXPERIMENTAL SECTION

4.1. Materials. Graphite powder, maleic anhydride (MA, 99.5%), choline chloride (ChCl, >98%), zinc chloride ($ZnCl_2$, >98%), ethylene glycol dimethacrylate (EGDMA, 99%), α,α'-azoisobutyronitrile (AIBN, 99%), and chloramphenicol (CAP, ≥98%) were purchased from Alfa Aesar. Graphene oxide (GO) was prepared by using the improved Hummer's method following a previous work.[36] VImBr was prepared according to a previous work.[37] The other solvents and chemicals of analytical grade were used as received. Deionized (DI) water was used in all of the experiments.

4.2. Characterizations. Thermogravimetric analysis (TGA) was performed with a Setaram Labsys Evo S60/58988 thermoanalyzer (France) under a nitrogen flow. The temperature range was set from 50 to 800 °C with a heating rate of 10 °C/min. Fourier transform infrared (FTIR) spectra were obtained by using a Bruker Tensor 27 (Germany) spectrometer in the 4000−500 cm^{-1} wavenumber. The crystallographic states of MS and PFA/MS hybrids were measured by a Shimadzu 6100 X-ray diffractometer (Japan) in the 2θ range of 5−80°. The surface morphologies of materials were observed by scanning electron microscopy (SEM) connected with an energy-dispersive X-ray (EDX) spectrometer (Hitachi JEOL-JSM-6700F system, Japan). Raman spectra

https://doi.org/10.1021/acsomega.3c02839
ACS Omega 2023, 8, 25385−25391

were examined with a LabRAM spectrometer (HORIBA Jobin Yvon, Edison, NJ) using a 785 nm diode laser. A Micromeritics 2020 volumetric adsorption analyzer system was used for measuring the BET surface area and pore-size distribution of MIP-rGO. HPLC analysis was performed on an HPLC Jasco LC-4000 system (Japan) with an ultraviolet (UV) L-4070 detector at a wavelength of 278 nm and an Apollo C18 column (250 mm × 4.6 mm, 5 μm) at 25 °C. The mobile phase was a mixture of pentane-1-sulfonic acid sodium salt (12 mM): acetonitrile (28:72 v/v) with a flow rate of 1.2 mL/min and an injection volume of 5 μL.

For electrochemical measurements, MIP-rGO-based electrodes were fabricated and tested for the electrochemical detection of CAP under ambient conditions using a potentiostat-galvanostat (VSP, BioLogic-Science Instruments, France) in alkaline media. A conventional three-electrode system was used with a platinum wire and Ag/AgCl (3 M NaCl) as counter and reference electrodes, respectively.

4.3. Covalent Functionalization of Maleic Anhydride onto rGO. GO was thermally annealed at 350 °C under an inert atmosphere to obtain rGO. DES was prepared from the mixture of $ZnCl_2$ and ChCl as described in our previous work.[38] First, MA (300 mg) was dissolved in DI water (3.0 mL) and the resulting solution was added to the mixture of rGO (100 mg) and DES (3.0 g). The reaction was allowed to occur at 60 °C for 2 h in an ultrasonic bath (GTSonic 150 W) at the frequency of 40 kHz. The solid material was separated and washed several times with DI water to remove adsorbed DES and unreacted MA. Finally, the nanocomposite was obtained after drying in a vacuum oven until constant weight and named as MA-rGO.

4.4. Anchoring of 3-Propyl-1-vinylimidazolium on MA-rGO. MA-rGO (50 mg) was dispersed in 100 mL of KOH (10 mM) solution. Then, VImBr (200 mg) was added to this dispersion and the ionic exchange process was initiated by stirring the resulting mixture at 50 °C for 5 h. The solid material was filtered, washed with DI water, and dried under vacuum at 45 °C until a constant weight, and named as VIm-rGO.

4.5. Polymerization of 3-Propyl-1-vinylimidazolium Units. VIm-rGO (80 mg), CAP (32 mg), and EGDMA (65 mg) were mixed and dispersed into 40 mL of a methanol/water (4:1, v/v) cosolvent system. The resulting mixture was continuously stirred under nitrogen flow at room temperature for 1 h. Subsequently, a deoxygenated solution of AIBN (60 mmol) was injected into this mixture and the reaction was further conducted at 60 °C for another 12 h. The solid product was collected and washed with DI water and ethanol. Finally, CAP templates were eluted by methanol to obtain a covalently functionalized molecularly imprinted polymer on the rGO surface (MIP-rGO) after drying under vacuum at 45 °C overnight. Moreover, a nonmolecularly imprinted polymer NIP-rGO was prepared using the same procedure without involving the CAP template for the comparison study.

4.6. Preparation of the Electrode. MIP-rGO was dispersed in ethanol (10 mg/mL) under sonication for 30 min. Then, 20 μL of a mixture was dropped on a glass carbon electrode (GCE) and left for drying to form a thin layer with an approx. area of 7.07 mm^2. Nafion-117 was used as a binder for the preparation of the electrode.

■ ASSOCIATED CONTENT

Supporting Information

The Supporting Information is available free of charge at https://pubs.acs.org/doi/10.1021/acsomega.3c02839.

SEM images; influence of interferences on the peak current of CAP; recovery capacity of CAP in real honey sample; and comparison of LOD toward CAP with previously reported literature (PDF)

■ AUTHOR INFORMATION

Corresponding Authors

Xuan Thang Cao − *Faculty of Chemical Engineering, Industrial University of Ho Chi Minh City, Ho Chi Minh City 700000, Vietnam;* orcid.org/0000-0002-4481-9814; Email: caoxuanthang@iuh.edu.vn

Subodh Kumar − *Department of Inorganic Chemistry, Faculty of Science, Palacký University Olomouc, 771 46 Olomouc, Czech Republic;* orcid.org/0000-0001-8872-2785; Email: subodh.kumar@upol.cz

Authors

Thi Nhat Thang Nguyen − *Faculty of Chemical Engineering, Industrial University of Ho Chi Minh City, Ho Chi Minh City 700000, Vietnam*

Nam Thi Pham − *Institute for Tropical Technology, Vietnam Academy of Science and Technology, Ha Noi 100000, Vietnam*

Dai-Hung Ngo − *Thu Dau Mot University, Thu Dau Mot City, Binh Duong 820000, Vietnam*

Complete contact information is available at: https://pubs.acs.org/10.1021/acsomega.3c02839

Notes

The authors declare no competing financial interest.

■ ACKNOWLEDGMENTS

This research was supported by the Industrial University of Ho Chi Minh City. S.K. acknowledges financial support from institutional sources of the Department of Inorganic Chemistry, Palacký University Olomouc, Czech Republic.

■ REFERENCES

(1) Mehta, J.; Dorst, B. V.; Rouah-Martin, E.; Herrebout, W.; Scippo, M.-L.; Blust, R.; Robbens, J. *In vitro* selection and characterization of DNA aptamers recognizing chloramphenicol. *J. Biotechnol.* **2011**, *155*, 361−369.

(2) Schirmer, C.; Meisel, H. Molecularly imprinted polymers for the selective solid-phase extraction of chloramphenicol. *Anal. Bioanal. Chem.* **2008**, *392*, 223−229.

(3) Berendsen, B.; Stolker, L.; Jong, Jd.; Nielen, M.; Tserendorj, E.; Sodnomdarjaa, R.; Cannavan, A.; Elliott, C. Evidence of natural occurrence of the banned antibiotic chloramphenicol in herbs and grass. *Anal. Bioanal. Chem.* **2010**, *397*, 1955−1963.

(4) Girardi, C.; Odore, R. Pharmacological treatments and risks for the food chain. *Vet. Res. Commun.* **2008**, *32*, S11−S18.

(5) Zhang, Q.; Zhou, Q.; Yang, L.; Wang, X.; Zheng, Y.; Bao, L. Covalently bonded aptamer-functionalised magnetic mesoporous carbon for high-efficiency chloramphenicol detection. *J. Sep. Sci.* **2020**, *43*, 2610−2618.

(6) Ali, I.; Aboul-Enein, H. Y.; Gupta, V. K.; Singh, P.; Negi, U. Analyses of chloramphenicol in biological samples by HPLC. *Anal. Lett.* **2009**, *42*, 1368−1381.

(7) Khoshbin, Z.; Verdian, A.; Housaindokht, M. R.; Izadyar, M.; Rouhbakhsh, Z. Aptasensors as the future of antibiotics test kits-A

case study of the aptamer application in the chloramphenicol detection. *Biosens. Bioelectron.* **2018**, *122*, 263−283.
(8) Liu, Y.; Yan, K.; Okoth, O. K.; Zhang, J. A label-free photoelectrochemical aptasensor based on nitrogen-doped graphene quantum dots for chloramphenicol determination. *Biosens. Bioelectron.* **2015**, *74*, 1016−1021.
(9) Borowiec, J.; Wang, R.; Zhu, L.; Zhang, J. Synthesis of nitrogen-doped graphene nanosheets decorated with gold nanoparticles as an improved sensor for electrochemical determination of chloramphenicol. *Electrochim. Acta* **2013**, *99*, 138−144.
(10) Lai, K.; Zhang, Y.; Du, R.; Zhai, F.; Rasco, B. A.; Huang, Y. Determination of chloramphenicol and crystal violet with surface enhanced Raman spectroscopy. *Sens. Instrumen. Food Qual. Saf.* **2011**, *5*, 19−24.
(11) Ferguson, J.; Baxter, A.; Young, P.; Kennedy, G.; Elliott, C.; Weigel, S.; Gatermann, R.; Ashwin, H.; Stead, S.; Sharman, M. Detection of chloramphenicol and chloramphenicol glucuronide residues in poultry muscle, honey, prawn and milk using a surface plasmon resonance biosensor and Qflex kit chloramphenicol. *Anal. Chim. Acta* **2005**, *529*, 109−113.
(12) Amjadi, M.; Jalili, R.; Manzoori, J. L. A sensitive fluorescent nanosensor for chloramphenicol based on molecularly imprinted polymer-capped CdTe quantum dots. *Luminescence* **2016**, *31*, 633−639.
(13) Wu, S.; Zhang, H.; Shi, Z.; Duan, N.; Fang, C. C.; Dai, S.; Wang, Z. Aptamer-based fluorescence biosensor for chloramphenicol determination using upconversion nanoparticles. *Food Control.* **2015**, *50*, 597−604.
(14) Liu, T.; Xie, J.; Zhao, J.; Song, G.; Hu, Y. Magnetic chitosan nanocomposite used as cleanup material to detect chloramphenicol in milk by GC-MS. *Food Anal. Methods* **2014**, *7*, 814−819.
(15) Tian, W.; Gao, L.; Zhao, Y.; Peng, W.; Chen, Z. Simultaneous determination of metronidazole, chloramphenicol and 10 sulfonamide residues in honey by LC−MS/MS. *Anal. Methods* **2013**, *5*, 1283−1288.
(16) Boyd, B.; Björk, H.; Billing, J.; Shimelis, O.; Axelsson, S.; Leonora, M.; Yilmaz, E. Development of an improved method for trace analysis of chloramphenicol using molecularly imprinted polymers. *J. Chromatogr. A* **2007**, *1174*, 63−71.
(17) Alizadeh, T.; Ganjali, M. R.; Zare, M.; Norouzi, P. Selective determination of chloramphenicol at trace level in milk samples by the electrode modified with molecularly imprinted polymer. *Food Chem.* **2012**, *130*, 1108−1114.
(18) Xie, Y.; Zhao, M.; Hu, Q.; Cheng, Y.; Guo, Y.; Qian, H.; Yao, W. Selective detection of chloramphenicol in milk based on a molecularly imprinted polymer−surface-enhanced Raman spectroscopic nanosensor. *J. Raman Spectrosc.* **2017**, *48*, 204−210.
(19) Schirmer, C.; Meisel, H. Synthesis of a molecularly imprinted polymer for the selective solid-phase extraction of chloramphenicol from honey. *J. Chromatogr. A* **2006**, *1132*, 325−328.
(20) Boyd, B.; Bjork, H.; Billing, J.; Shimelis, O.; Axelsson, S.; Leonora, M.; Yilmaz, E. Development of an improved method for trace analysis of chloramphenicol using molecularly imprinted polymers. *J. Chromatogr. A* **2007**, *1174*, 63−71.
(21) Zhu, N.; Han, S.; Gan, S.; Ulstrup, J.; Chi, Q. Graphene paper doped with chemically compatible prussian blue nanoparticles as nanohybrid electrocatalyst. *Adv. Funct. Mater.* **2013**, *23*, 5297−5306.
(22) Hoa, L. T.; Sun, K. G.; Hur, S. H. Highly sensitive non-enzymatic glucose sensor based on Pt nanoparticle decorated graphene oxide hydrogel. *Sens. Actuators, B* **2015**, *210*, 618−623.
(23) Gupta, S.; Smith, T.; Banaszak, A.; Boeckl, J. Graphene quantum dots electrochemistry and sensitive electrocatalytic glucose sensor development. *Nanomaterial* **2017**, *7*, No. 301.
(24) Weaver, C. L.; Li, H.; Luo, X.; Cui, X.T. A graphene oxide/conducting polymer nanocomposite for electrochemical dopamine detection: origin of improved sensitivity and specificity. *J. Mater. Chem. B* **2014**, *2*, 5209−5219.
(25) Cardoso, A. R.; Marques, A. C.; Santos, L.; Carvalho, A. F.; Costa, F. M.; Martins, R.; Sales, M.G.F.; Fortunato, E. Molecularly-imprinted chloramphenicol sensor with laser-induced graphene electrodes. *Biosens. Bioelectron.* **2019**, *124*−*125*, 167−175.
(26) Beduk, T.; Lahcen, A. A.; Tashkandi, N.; Salama, K.N. One-step electrosynthesized molecularly imprinted polymer on laser scribed graphene bisphenol a sensor. *Sens. Actuators, B* **2020**, *314*, No. 128026.
(27) Jia, B. J.; He, X.; Cui, P. L.; Liu, J. X.; Wang, J.P. Detection of chloramphenicol in meat with a chemiluminescence resonance energy transfer platform based on molecularly imprinted graphene. *Anal. Chim. Acta* **2019**, *1063*, 136−143.
(28) Shinde, S. S.; Sami, A.; Lee, J.-H. Electrocatalytic hydrogen evolution using graphitic carbon nitride coupled with nanoporous graphene co-doped by S and Se. *J. Mater. Chem. A* **2015**, *3*, 12810−12819.
(29) Yam, K. H.; Guo, N.; Jiang, Z.; Li, S.; Zhang, C. Graphene-Based Heterogeneous Catalysis: Role of Graphene. *Catalysts* **2020**, *10*, No. 53.
(30) Kumar, N. A.; Choi, H.-J.; Shin, Y. R.; Chang, D. W.; Dai, L.; Baek, J.-B. Polyaniline-grafted Reduced graphene oxide for efficient electrochemical supercapacitors. *ACS Nano* **2012**, *6*, 1715−1723.
(31) Karousis, N.; Sandanayaka, A. S. D.; Hasobe, T.; Economopoulos, S. P.; Sarantopoulou, E.; Tagmatarchis, N. Graphene oxide with covalently linked porphyrin antennae: Synthesis, characterization and photophysical properties. *J. Mater. Chem.* **2011**, *21*, 109−117.
(32) Le, C. M. Q.; Cao, X. T.; Tu, T. T. K.; Lee, W.-K.; Lim, K. T. Facile covalent functionalization of carbon nanotubes via Diels-Alder reaction in deep eutectic solvents. *Appl. Surf. Sci.* **2018**, *450*, 122−129.
(33) Nguyen, T. H. A.; Tran, T. Q. N.; Nguyen, T. N. T.; Van, T. K.; Ngo, D.-H.; Kumar, S.; Cao, X. T. Deep eutectic solvent assisted synthesis of poly(furfuryl alcohol) grafted carbon nanotubes: a metal free electrocatalyst for non-enzymatic glucose detection. *New J. Chem.* **2022**, *46*, 15799−15803.
(34) Jakubec, P.; Urbanová, V.; Medříková, Z.; Zbořil, R. Advanced Sensing of Antibiotics with Magnetic Gold Nanocomposite: Electrochemical Detection of Chloramphenicol. *Chem.− A Eur. J.* **2016**, *26*, 14279−14284.
(35) El-Hallag, I. S.; El-Nahass, M. N.; Youssry, S. M.; Kumar, R.; Abdel-Galeil, M. M.; Matsuda, A. Facile *in-situ* simultaneous electrochemical reduction and deposition of reduced graphene oxide embedded palladium nanoparticles as high performance electrode materials for supercapacitor with excellent rate capability. *Electrochim. Acta* **2019**, *314*, 124−134.
(36) Le, M.-Q.C.; Cao, X. T.; Lee, W. K.; Hong, S.-S.; Lim, K. T. Fabrication and adsorption properties of novel magnetic graphene oxide composites for removal of methylene blue. *Mol. Cryst. Liq. Cryst.* **2017**, *644*, 160−167.
(37) Jana, S.; Vasantha, V. A.; Stubbs, L. P.; Parthiban, A.; Vancso, J.G. Vinylimidazole-based asymmetric ion pair comonomers: Synthesis, polymerization studies and formation of ionically crosslinked PMMA. *J. Polym. Sci., Part A: Polym. Chem.* **2013**, *51*, 3260−3273.
(38) Cao, T. P.; Hang, C. N.; Vu Quang, H.; Kabtamu, D. M.; Kumar, S.; Nguyen, V. C.; Cao, X. T. Catalyst-free synthesis of poly (furfuryl alcohol) using deep eutectic solvents. *New J. Chem.* **2022**, *46*, 3786−3793.

https://doi.org/10.1021/acsomega.3c02839
ACS Omega 2023, 8, 25385−25391